EUROPEAN ORGANIZATION FOR NUCLEAR RESEARCH
European Laboratory for Particle Physics

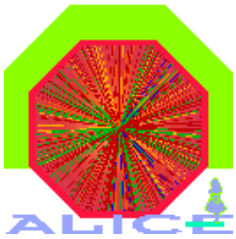

Internal Note/Physics
ALICE reference number
ALICE-INT-2005-018 version 1.0
Institute reference number
[-]
Date of last change
August 22, 2005

Key words: heavy flavor
ALICE muon spectrometer

Measuring the *b*-Meson Production Cross Section in 5.5 TeV Pb-Pb Collisions Using Semileptonic Decay Muons

Authors:

Rachid Guernane[1], Philippe Crochet[2], Andreas Morsch[3], Ermanno Vercellin[1]

[1] Università di Torino/INFN, Torino, Italy
[2] LPC, Univ. Blaise Pascal and CNRS-IN2P3, Aubière, France
[3] CERN, Geneva, Switzerland

Abstract:

A feasibility study for the measurement of the *b*-hadron production cross section in central Pb-Pb collisions at LHC using semimuonic decay muons is presented.

1 Introduction

As an intrinsically perturbative phenomenon heavy quark production is an important benchmark for testing QCD and parton model concepts. At hadron colliders the ratio between the measured differential b-hadron production cross-section and the central theory prediction is typically a factor 2-3. Whereas measurements by UA1 at the Sp$\overline{\text{p}}$S collider lie inside the error band of the predictions comparison of early TeVatron data [1, 2, 3, 4] with theory have led to the pessimistic conclusion of a disagreement with pQCD. More recently, an accurate implementation of up-to-date hadronization effects have decreased the ratio between data and central theory value from $2.9 \pm 0.2 \pm 0.4$ [5] to $1.7 \pm 0.5 \pm 0.5$ [6]. In the context of heavy ion collisions, open heavy quark production is a well suited probe to measure the incoming gluon structure functions and more particularly gluon shadowing effects in nuclei [7, 8]. Moreover, due to their long lifetime heavy quarks can live through the thermalization phase of a QGP and therefore carry information about the deconfined phase [9]. Measuring the beauty hadron cross-section down to very low p_{t} is essential since in this region the bulk of the cross-section is sitting and since it will be influenced by non-perturbative effects which can be different in pp and AA collisions. The measurement of the beauty quark yield in the same kinematic region as for the Υ measurement will provide a valuable reference against which to compare Υ production in order to observe a possible suppression in AA collisions.

In this note, our purpose is to present a study of the ALICE muon spectrometer capabilities to measure the inclusive b-hadron production cross section in the (di)muon channel. It is based on the latest Monte Carlo simulations of the production cross sections as well as kinematic distributions of decay muons from heavy flavor production in heavy ion collisions.

2 Heavy quark hadroproduction phenomenology

Unlike shower Monte Carlos, analytic calculations include higher order corrections to the hard scattering processes. In the analysis presented hereafter, the PYTHIA event generator [10] has been used. To improve its predictive power the parameters have been tuned to reproduce the heavy quark kinematics from the analytic re-summation calculations obtained by Mangano *et al.* [11]. In the following sections, after briefly introducing the pQCD calculation (section 2.1), we describe the PYTHIA model (section 2.2) detailing the choice of the different non-pertubative parameters (section 2.3).

2.1 Perturbative QCD calculation

Heavy quark hadroproduction cross sections can be calculated in perturbative QCD according to the factorization theorem [12]

$$\mathrm{d}\sigma_{\mathrm{AB}}(s) = \sum_{i,j} \int \mathrm{d}x_{\mathrm{A}}\ \mathrm{d}x_{\mathrm{B}}\, \mathrm{d}\,\hat{\sigma}_{\mathrm{ij}}\ (x_{\mathrm{A}} x_{\mathrm{B}} s,\ m^2, \mu_{\mathrm{R}}^2)\, f_{\mathrm{i}}^{\mathrm{A}}\ (x_{\mathrm{A}}, \mu_{\mathrm{F}})\ f_{\mathrm{j}}^{\mathrm{B}}(x_{\mathrm{B}}, \mu_{\mathrm{F}}), \tag{1}$$

where $\sqrt{s}$ is the center-of-mass energy of the initial hadron collision system, $f_{\mathrm{i}}^{\mathrm{A}}$ are the structure functions measuring the probability of the ith parton in hadron A to carry fractional momentum x_{A}, m is the heavy quark mass, μ_{R} and μ_{F} are the renormalization and factorisation scales and $\mathrm{d}\,\hat{\sigma}_{\mathrm{ij}}$ is the total partonic cross section of the process ij $\rightarrow Q\bar{Q}X$ at the effective center of mass energy $\hat{s} = x_{\mathrm{A}}\, x_{\mathrm{B}}\, s$. $\mathrm{d}\,\hat{\sigma}_{\mathrm{ij}}$ is computed within the framework of perturbative QCD as a power series expansion in the strong coupling constant $\alpha_{\mathrm{S}}(m^2)$. Mangano, Nason, and Ridolfi

present in Ref. [11] a fully exclusive partonic differential cross section calculation including all the relevant partonic subprocesses:

$$q\bar{q} \rightarrow Q\bar{Q}, \quad \alpha_S^2, \alpha_S^3 \tag{2a}$$
$$g\bar{g} \rightarrow Q\bar{Q}, \quad \alpha_S^2, \alpha_S^3 \tag{2b}$$
$$q\bar{q} \rightarrow Q\bar{Q}g, \quad \alpha_S^3 \tag{2c}$$
$$g\bar{g} \rightarrow Q\bar{Q}g, \quad \alpha_S^3 \tag{2d}$$
$$g\bar{q} \rightarrow Q\bar{Q}g, \quad \alpha_S^3 \tag{2e}$$

Representative Feynman diagrams for lowest order "flavor creation" processes (cf. equations (2a) and (2b)) are shown in figure 1 while higher order graphs are displayed in figure 2. Unlike LO processes [1], NLO processes (cf. equations (2c), (2d), and (2e)) can produce characteristic quasi collinear heavy quark pair recoiling against the light parton left over in the hard scattering.

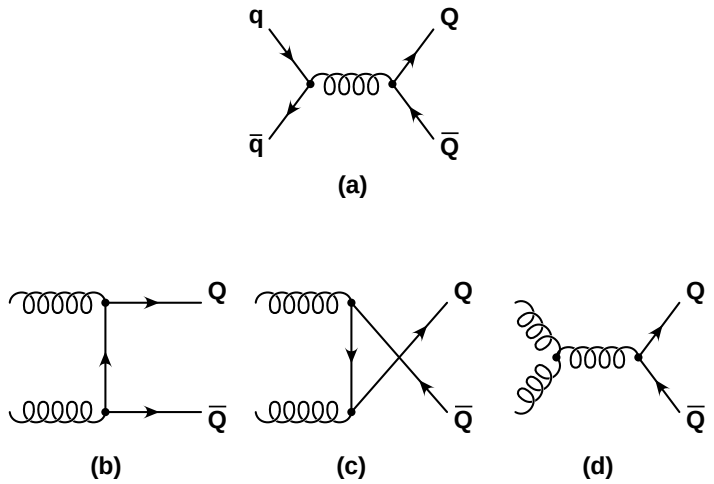

Fig. 1: Feynman graphs for lowest order "flavor creation" processes, *e.g.* quark-antiquark annihilation (a) and gluon fusion (b), (c), and (d).

2.2 Model description: the PYTHIA approach

PYTHIA is a leading-log Monte-Carlo model with respect to heavy flavor production. This means that the hard scattering only involves $2 \rightarrow 2$ QCD processes. These lowest order diagrams are simulated using matrix elements taking into account correctly the quark mass. Higher order processes are only present through the simulation of initial and final state shower evolution giving rise to heavy quark production through the so called flavor excitation and gluon splitting processes. At LHC these processes represent an important contribution and can be simulated using the parton shower approach by selection events containing heavy quark pairs from a full sample of $2 \rightarrow 2$ QCD processes. In Pythia the latter are simulated in the massless approximation, in which the parton-parton differential cross section diverges as the p_t of the hard scattering tends toward 0. A regularization is introduced applying a large enough cut $p_{t,min}^{hard}$ ‡‡.

[1] QCD $2 \rightarrow 2$ give rise to a small net transverse momentum of the $Q\bar{Q}$ pair and $p_t^Q \simeq \langle m_Q \rangle$.

‡‡ p_t^{hard} is the transverse momentum of the outgoing partons in the rest frame of the hard interaction.

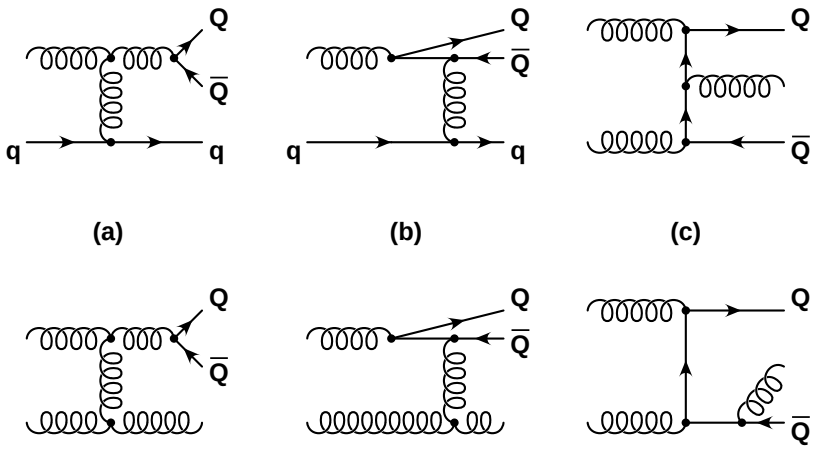

Fig. 2: Feynman diagrams of next-to-leading order heavy quark production for: (a) final state "gluon splitting" into a $Q\bar{Q}$ pair, (b) higher order flavor excitation, and (c) $\mathcal{O}(\alpha_s^2)$ graph can radiate gluons.

Single-inclusive observables for heavy quark production depend on the $p_{\mathrm{t}\,min}^{\mathrm{hard}}$ value, consequently the tuning of PYTHIA consists in adjusting the $p_{\mathrm{t,min}}^{\mathrm{hard}}$ to reproduce NLO calculations, all other non-perturbative parameters (described in the next section) being fixed. Finally, 2.1 GeV/c and 2.75 GeV/c were chosen for charm and beauty respectively [13].

2.3 Non-perturbative ingredients

2.3.1 Primordial transverse momentum

Initial state partons entering the hard scattering process are assigned a random transverse momentum $k_\perp$ drawn from a Gaussian distribution. The width $\langle k_\perp^2 \rangle = \sigma_{k_\perp}^2$ of the Gaussian which increases with $\sqrt{s}$ is a free parameter that should be adjusted from the data. As no data are available at LHC energies, we do not use the default $1\,\mathrm{GeV}^2$ value and tuned it to reproduce NLO differential cross-section shapes. The final values are $1.3\,\mathrm{GeV}^2$ for charm and $2.04\,\mathrm{GeV}^2$ for beauty [13].

2.3.2 Structure function

In our PYTHIA-based calculation, the CTEQ 4L leading order parton distribution function [14] is used. Changing the structure function modifies the relative fraction of flavor excitation mechanism. This choice is basically motivated by the good agreement of the PYTHIA prediction with available inclusive beauty production measurements[15].

Nuclear shadowing

Structure functions measured on bound nucleons differ from those of free nucleons [16]. In the low x region ($x \lesssim 0.01$), nuclear effects known as "shadowing" tend to deplete the nuclear parton distribution. In the simulation, we used the EKS98 modification of the nuclear parton density function valid in the region $10^{-6} \leq x \leq 1$, $Q^2 \geq 2.25\,\mathrm{GeV}^2$ [17].

2.3.3 Heavy quark fragmentation and hadronization

Heavy flavors in the final state of the hard process are hadronized using the Lund string fragmentation model [18]. The non-perturbative hadronization of a string consists in $q\bar{q}$ pair production in the color field which arrange to form subsequent hadrons. The probability distribution for generating a hadron which carries a fraction z of the original quark momentum is given by a fragmentation function f(z), where

$$z = \frac{E^{\mathrm{H}} + p_{||}^{\mathrm{H}}}{E^{\mathrm{Q}} + p^{\mathrm{Q}}} \tag{3}$$

where $p_{||}^{\mathrm{H}}$ is the momentum of the hadron in the direction of the quark Q. Fig. 3 compares the shapes of heavy quark string fragmentation functions. The Lund string fragmentation function is rather different from the Peterson *et al.* form [19]. In the context of string fragmentation, the perturbatively produced heavy quarks are connected to the beam remnants by color singlet strings and thus can gain energy and momentum through soft interactions resulting in $z > 1$ values. It is worth noting that beam-drag effect is not directly accessible experimentally, but only as a discrepancy between the shape of perturbatively calculated quark distributions and the data.

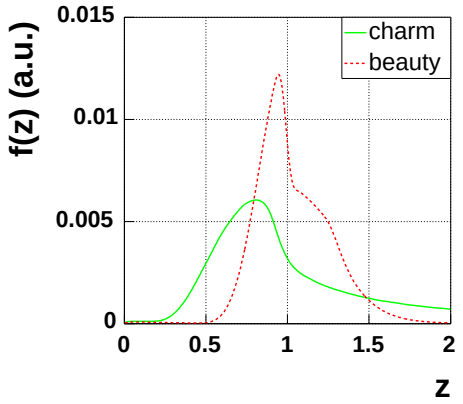

Fig. 3: Lund string fragmentation function for charm and beauty quark. Note that z has a non zero probability to be larger than 1 due to beam-drag effects.

The beauty quark has a harder fragmentation than the charm which means that, on average, b-mesons carry a larger fraction of the momentum of the original quarks. This results in a harder transverse momentum spectrum of muons from beauty quarks than from charm quarks. PYTHIA calculation of the p_{t} spectra of beauty quarks, B mesons and muons from b-meson decays is plotted in Fig. 4, together with the corresponding spectra for charm.

2.3.4 Semileptonic decay of heavy flavored hadrons

Charm and beauty hadrons formed in the fragmentation process decay semileptonically via the weak force. As indicated in the diagram for semileptonic b-meson decay in Fig. 5, a b-quark turns into a c quark through the emission of a virtual W^- boson which subsequently decays to a negatively charged lepton plus an antineutrino. In PYTHIA, these decays are treated using the

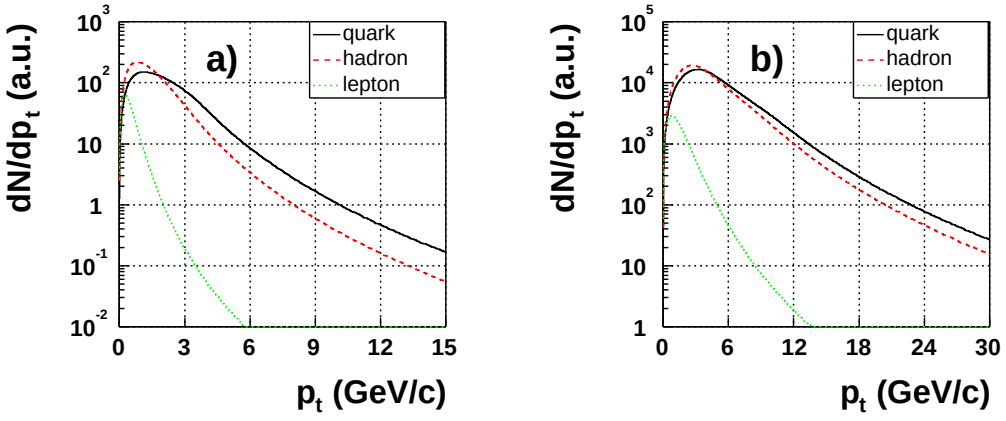

Fig. 4: $p_{\rm t}$ spectra of quarks, mesons and muons from (a) charm and (b) beauty production predicted by PYTHIA.

naive V–A weak decay matrix elements. In this "spectator model", the heavy quark in a meson is considered to be independent of the light quark allowed to decay as a free particle with the simple V–A weak current [20].

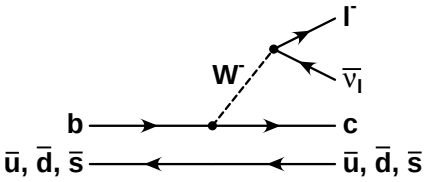

Fig. 5: Feynman diagram depicting the semileptonic (spectator) decay of a $\overline{B}$ meson into a lepton plus a charmed meson.

3 Beauty production measurement with the ALICE forward muon spectrometer

After having described the different components of the heavy quark cross section calculations, we will now detail the muon spectrometer capabilities for beauty measurements. Above all, the muon arm will be able to detect both single and di-muons. The latter allow an in-depth study of $\rm Q\bar{Q}$ correlations sensitive to QCD specific predictions as explained in the next sections.

3.1 Single inclusive heavy quark production

Single inclusive differential cross-section measurements are motivated by the following features:

- Infrared and collinear divergences in the phase-space integration of the single inclusive differential cross section formulae cancel properly. A theoretical calculation is then more easily accessible [21];

- Statistics available will be higher since only one muon from the heavy quark decay has to pass the acceptance. It is worth to note, however, that in practice the statistics might be limited by the available bandwidth, by the running and trigger strategies which will be adopted.

All these arguments justify the one-particle inclusive differential cross-section measurement to be the starting point of an experimental heavy quark physics program as recently published by PHENIX at RHIC collider [22].

3.2 Heavy quark correlations: a probe for higher-order QCD corrections

Our ability to measure both muons from the heavy quark pair decay offer additional information as compared to single inclusive cross-sections to test the QCD dynamics.

- **Azimuthal angle, $\delta\phi$:** defined as the angle between the projections of the muon pair momenta onto the transverse plane with respect to the beam direction, the azimuth angle is peaked at 180° for leading-log processes. Measuring the transverse opening angle distribution is a direct indication of the importance of higher-order contributions. Moreover, comparing measurements with parton shower model prediction could constrain the model in describing flavor excitation and gluon splitting.

- **Transverse momentum asymmetry, A:** for lowest order $\left|\frac{p_{\rm t}^{Q} - p_{\rm t}^{\bar{Q}}}{p_{\rm t}^{Q} + p_{\rm t}^{\bar{Q}}}\right|$ should be 0 due to momentum conservation demanding heavy quarks to be emitted back-to-back balanced in $p_{\rm t}$. It's no longer the case for higher order graphs giving very different $\rm Q\bar{Q}$ pair topologies, *i.e.* gluon splitting can produce very collimated heavy quarks recoiling against a light parton jet.

- **Rapidity correlation, δy:** at leading order in pQCD, $\rm Q\bar{Q}$ pairs are produced through $q\bar{q}$ annihilation and gluon fusion (cf. Fig. 1). The annihilation process proceeds exclusively through the s-channel and leads to a rapidity correlation $\mathrm{d}\sigma/\mathrm{d}\hat{s} \sim (\cosh\delta y)^{-2}$ at large $\delta y = y_{\rm Q} - y_{\bar{\rm Q}}$ [23]. The gluon fusion process includes t-channel exchange diagrams that enhance the contribution from final states where the Q and $\bar{\rm Q}$ are produced at small angles (in the center-of-mass) with respect to the beam and leads to a less-pronounced rapidity correlation, $\mathrm{d}\sigma/\mathrm{d}\hat{t} \sim (\cosh\delta y)^{-1}$. For either process, the partonic cross section is suppressed as the rapidity difference increases and it is expected that a $\rm Q\bar{Q}$ pair will be found closely separated in rapidity. For NLO $\rm Q\bar{Q}$ processes, pair creation with "gluon emission" and "flavor excitation" lead to a broadening of the δy distribution while the gluon splitting process leads to an enhancement for $\delta y \sim 0$.

  In Fig. 6, we show rapidity correlations between muons originating from $\rm Q\bar{Q}$ decays. In Figs. 6(b) and (d), rapidity difference distributions between muons when one of the two muons is in the muon spectrometer geometric acceptance from charm and beauty decays respectively are presented. Muon rapidity correlation is stronger for beauty decays with a standard deviation of roughly 1.5 units (2 rapidity units for charm).

  Strong rapidity correlation of muons from beauty decays makes the ALICE forward muon spectrometer design particularly well suited to efficiently collecting $b\bar{b}$ pairs since it implies that if a b quark is detected in the forward region there is a high probality that the $\bar{b}$ is also forward. $b\bar{b}$ acceptance is detailed in Table 1.

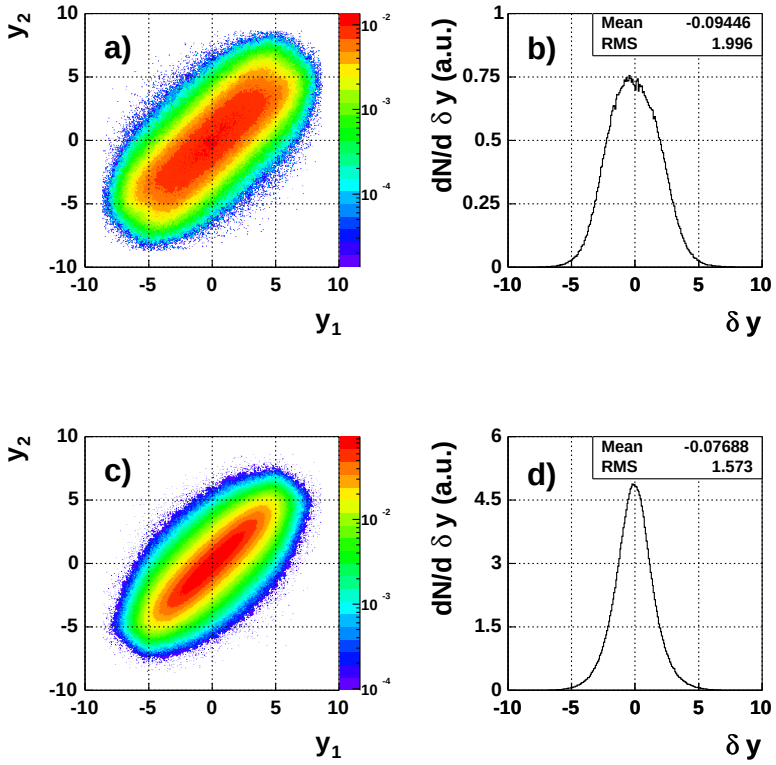

Fig. 6: Dimuon rapidity distributions for (a) charm and (c) beauty decays. Rapidity difference δy distributions when one muon is in the muon arm acceptance for (b) charm and (d) beauty.

While very promising, neither azimuthal nor transverse momentum correlations have been exploited in the present analysis to enhance heavy quark signals.

3.3 Heavy quark production rates at the LHC

3.3.1 ALICE benchmark heavy quark cross sections in p-p collisions

c and b-quark are expected to be copiously produced from initial nucleon-nucleon interactions at the LHC. Precise pp data are mandatory as a baseline for AA rates. In the following, AA interactions will be considered as simple superpositions of pp collisions (cf. section 3.3.2). In Table 2, we quote relevant predictions of the cross sections [13] used in the muon analysis.

3.3.2 Heavy flavor production in heavy ion collisions

Open heavy quark production cross sections in heavy ion collisions (AB) are inferred from nucleon-nucleon (nn) ones in accordance with the Glauber multiple scattering model [24]. In the Glauber approximation, the average hard scattering yields per collision scale with the number of nucleon-nucleon collisions (the so-called "binary scaling") according to[2]:

$$\langle \mathcal{N}_{\rm AB}^{\rm hard} \rangle (\mathrm{b}) \simeq \langle \mathcal{N}_{\rm coll} \rangle (\mathrm{b}) \times \mathcal{N}_{\rm nn}^{\rm hard}, \tag{4}$$

[2]No nuclear effects on the hard process cross section are included.

Table 1: Muon arm detection efficiency breakdown for single muons and dimuons from charm and beauty. $A_{\mathbb{g}}$ stands for the muon arm geometrical acceptance, $A_{\mathbb{t}}$ for the fraction of trackable tracks, while $\varepsilon_{\mathbb{r}}$ is the tracking efficiency, $\varepsilon_{\mathbb{t}}^{\mathbb{L}}$ the low-p_{t} trigger efficiency, and $\varepsilon_{\mathbb{t}}^{\mathbb{H}}$ the hight-p_{t} trigger efficiency.

	$c\bar{c}$			$b\bar{b}$			
	μ^+	μ^-	$\mu^+\mu^-$	μ^+	μ^-	$\mu^+\mu^-$	$\mu^\pm\mu^\pm$
$A_{\mathbb{g}}$	0.130	0.127	0.035	0.122	0.122	0.050	0.031
$A_{\mathbb{t}}$	0.422	0.420	0.191	0.756	0.757	0.465	0.515
$\varepsilon_{\mathbb{r}}$	0.271	0.270	0.080	0.622	0.624	0.287	0.339
$\varepsilon_{\mathbb{t}}^{\mathbb{L}}$	0.130	0.133	0.021	0.530	0.540	0.171	0.233
$\varepsilon_{\mathbb{t}}^{\mathbb{H}}$	0.040	0.042	0.003	0.285	0.293	0.043	0.067

Table 2: Next-to-leading order total charm and beauty cross sections [mb] in p-p collisions at $\sqrt{s} = 5.5\,\mathrm{TeV}$ calculated with two extreme sets of recent parton distributions (to approach the theoretical error) and including nuclear effects (third row).

p.d.f.	MRST HO	CTEQ 5M1	EKS98
$\sigma_{c\bar{c}}$	5.9	7.4	
$\langle\sigma_{c\bar{c}}\rangle$	6.64		4.32
$\sigma_{b\bar{b}}$	0.19	0.22	
$\langle\sigma_{b\bar{b}}\rangle$	0.21		0.18

where $\langle\mathcal{N}_{\mathrm{coll}}\rangle$ is the average number of binary inelastic interactions in a AB collision written as:

$$\langle\mathcal{N}_{\mathrm{coll}}\rangle(\mathrm{b}) = \sigma_{\mathrm{nn}} \times \mathcal{T}_{\mathrm{AB}}(\mathrm{b}), \tag{5}$$

where σ_{nn} is the nucleon-nucleon inelastic cross section ($\sim 72\,\mathrm{mb}$ at LHC energies) and $\mathcal{T}_{\mathrm{AB}}(\mathrm{b})$ is the nuclear overlap function [25]. Hard process rate in nucleon-nucleon interactions $\mathcal{N}_{\mathrm{nn}}^{\mathrm{hard}}$ is given by $\sigma_{\mathrm{nn}}^{\mathrm{hard}}/\sigma_{\mathrm{nn}}$, $\sigma_{\mathrm{nn}}^{\mathrm{hard}}$ values in p-p collisions calculated at NLO in QCD are presented in Table 2. Eventually, using scaling parameters from Table 3, heavy flavor expected production rates in Pb-Pb collisions are presented in Table 4.

Table 3: Number of inelastic nucleon-nucleon collisions $\langle\mathcal{N}_{\mathrm{coll}}\rangle$ and nuclear overlap $\mathcal{T}_{\mathrm{PbPb}}$ for the 5 % most central PbPb and minimum bias reactions inferred from the Glauber model [26].

centrality bin	$\langle\mathcal{N}_{\mathrm{coll}}\rangle$	$\mathcal{T}_{\mathrm{PbPb}}\,[\mathrm{mb}^{-1}]$
$0 \div 5\,\%$	1876	26
M.B.	400	5.58

Table 4: Summary of heavy flavor production rates in Pb-Pb collisions with an average luminosity of $\mathscr{L}_{\text{Pb-Pb}} = 5 \times 10^{26}\,\text{cm}^{-2} \cdot \text{s}^{-1}$. Hard scattering cross sections including shadowing are taken from Table 2 and the Pb-Pb geometric cross section is taken to be 7.39 b.

Rates	$c\bar{c}$		$b\bar{b}$	
centrality bin	$0 \div 5\,\%$	M.B.	$0 \div 5\,\%$	M.B.
/collision	115.8	25.3	4.8	1.0
$/10^6$ s $[\times 10^{10}]$	2.1	9.3	0.09	0.4

3.4 Detector effects

Acceptance, detection efficiencies and resolution of the muon arm have been included from a detailed description predicated on a phase space discretization[3] of a full Geant 3.21 simulation [27].

3.4.1 Geometrical acceptance

Muon geometrical acceptance ($\text{A}_{\mathbb{g}}$) has been computed by applying simple pseudo-rapidity cuts corresponding to the geometric aperture of the spectrometer ($2.5 < \eta < 4$).

3.4.2 Muon tracking reconstruction

The muon tracking implements a maximum likelihood expectation maximization (MLEM) cluster finder and a Kalman filter track fitting [28]. Fig. 7(a) shows the transverse momentum resolution of muon tracks in nominal soft background level resulting from the merging of two central HIJING [29] events with gluon shadowing and jet quenching producing a charged particle density $\text{dN}/\text{d}\eta|_{\eta=0} = 6000$¶. Muon tracks of $p_{\text{t}>1.5\,\text{GeV/c}}$ have a relative p_{t} resolution better than 2 % and a reconstruction efficiency ($\varepsilon_{\mathbb{r}}$) for trackable tracks (fraction $\text{A}_{\mathbb{t}}$ of the tracks emitted in the spectrometer opening angle giving hits in 1 chamber (out of 2) of each tracking station 1-3, 3 chambers (out of 4) in stations 4-5 and 3 chammbers (out of 4) in trigger stations) of about 90 % with 10 % losses at the edges of the rapidity range (cf. Fig 7(b)). Reconstruction efficiencies for single and di-muons are summarized in Table 1.

3.4.3 Muon trigger efficiencies

In central Pb-Pb collisions, about eight low transverse momentum muons from π/K decays are expected to be emitted per event in the spectrometer angular aperture. To reduce the trigger probability to a reasonable level, a muon trigger signal is issued only if a track has a transverse momentum above a predefined threshold. Although trigger levels have been optimized for quarkonia measurements, in this analysis, we show that the low trigger transverse momentum cut-off of 1 GeV/c is enough to have a significant measurement of open beauty in the dimuon channel over the whole mass range. An additional analysis (sharp) cut of 1.5 GeV/c is finally applied to avoid distorsion of the trigger efficiency at low transverse momentum (cf. Fig. 7(c)). Low ($\varepsilon_{\mathbb{t}}^{\mathbb{L}}$) and high ($\varepsilon_{\mathbb{t}}^{\mathbb{H}}$) trigger cut efficiencies for single and muons pairs are given in Table 1.

[3] Arranged in look-up tables.

¶ Due to large uncertainties on charged particle multiplicity expected at the LHC and in order to base the spectrometer design on conservative values, the nominal background level includes a safety factor of two.

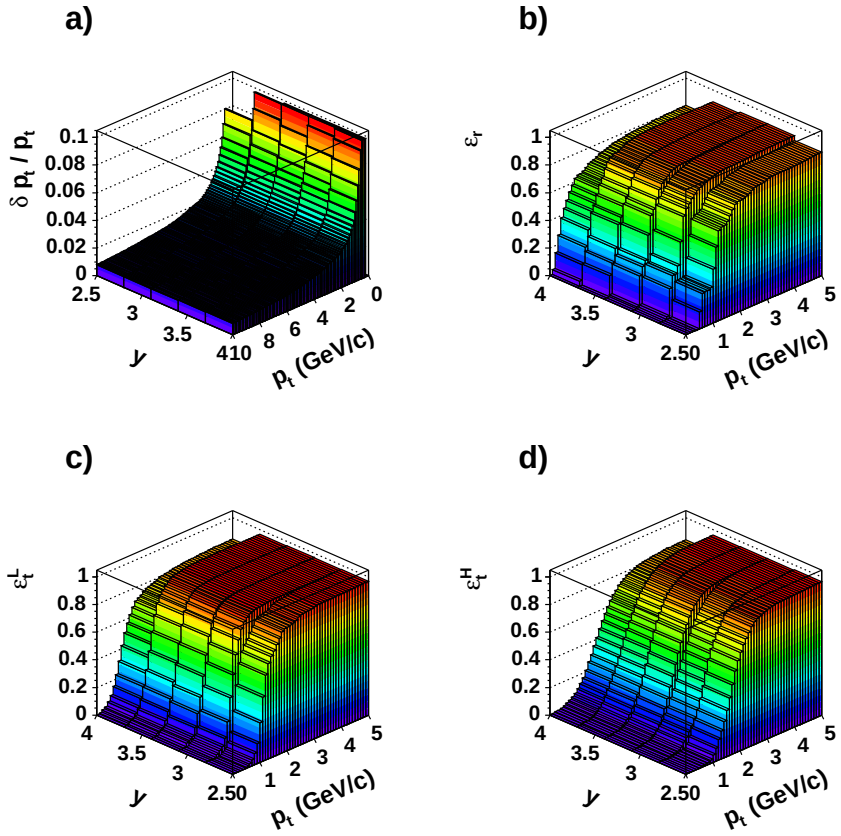

Fig. 7: ALICE forward muon spectrometer single track response in the (p_{t}, y) plane for nominal background condition calculated from a fast parametrisation based on detailed geometry simulation. Transverse momentum resolution (a), tracking reconstruction efficiency (b), low p_{t} (c) and high p_{t} (b) trigger efficiences are presented.

3.4.4 Global efficiencies

Finally, combining previously described efficiencies, we obtain total efficiencies both for single and muon pairs from heavy quark decays presented in Table 5. b-quark decays produce muons with larger transverse momentum as compared to charm resulting in sensibly better single track efficiencies.

3.5 Muon sources

Regarding beauty production, in addition to the direct semimuonic decay $B \to \mu\nu X$, second generation muons can also originate from cascade decay $B \to DX, D \to \mu\nu X'$. Relevant semimuonic branching ratio are shown in Table 6.

While charm semimuonic decays can only contribute to the unlike-sign dimuon sample, beauty decays through cascade chains are likely to produce both like-sign and opposite-sign dimuons as

Table 5: Global efficiencies for single and opposite sign muon pair data samples.

p_t^μ (GeV/c)	ε
$1.5 \div 3$	0.852
$3 \div 6$	0.899
$6 \div 9$	0.907
$9 \div 30$	0.933

$M_{\mu^+\mu^-}$ (GeV/c)	ε
$0 \div 5$	0.636
$5 \div 20$	0.723

$$\begin{aligned} B^+ &\to \overline{D^0}\,\ell_1^+\nu_\ell \\ &\quad\hookrightarrow \ell_2^-\,X' \\ \overline{B^0} &\to D^+\,\ell_3^-\,\overline{\nu_\ell} \\ &\quad\hookrightarrow \ell_4^+\,X'' \end{aligned} \tag{6}$$

B decays can therefore produce both same sign and opposite sign lepton pairs as follows: a combination of leptons ($\ell_1\ell_2$ and $\ell_3\ell_4$) from a single B[§] (refered to as BD_{same}), two leptons ($\ell_1\ell_3$) from primary B decays (BB_{diff}), two leptons ($\ell_2\ell_4$) from secondary decays (DD_{diff}) feed down from beauty to the open charm production[4], and a primary lepton from one B and a secondary lepton from the other B ($\ell_1\ell_4$ and $\ell_2\ell_3$ or BD_{diff}). Moreover mixing in the B^0–$\overline{B^0}$ system (cf. section 3.5.1) can change B charge producing same sign correlated BB_{diff} and DD_{diff} muon pairs.

Semileptonic decay muons from heavy flavors are *non-isolated i.e.* accompanied by hadronic jets. A full reconstruction of the initial heavy quark in the semimuonic decay channel is impossible due to undetected neutrinos. An opposite sign muon pair from a b chain decay has however an upper limit on its mass fixed by the initial b quark mass which can be used to identify this process. In practice, heavy flavor decays can be divided into two main topologically distinct contributions, b-chain decays of low mass and high transverse momentum dimuons (Fig. 8(a)) and muon pairs where the two muons originate from different quarks (Fig. 8(b)) emitted at large angles resulting in large invariant masses.

If a cut on the muon transverse momentum is applied, as it is the case in the following analysis, the secondary decays are heavily suppressed, as some fraction of the momentum has already been used up in the primary decay.

[§] Always opposite sign.
[4] Both same and opposite sign.

Table 6: Heavy hadron electroweak properties from PYTHIA (numbers quoted without error) and obtained by the LEPEWWG [30, 31] or quoted by the PDG [32].

Semi-muonic branching fractions

***c*-hadrons**			***b*-hadrons**		
D^+	0.172	0.102 ± 0.009	B^+	0.105	0.102 ± 0.009
D^0	0.077	0.065 ± 0.008	B^0	0.105	0.105 ± 0.008
D_s^+	0.080	$0.08 \pm^{0.06}_{0.05}$	$B_s^0 \to D_s^- \ell^+ \nu_\ell$	0.105	0.079 ± 0.024
Λ_c^+	0.045	0.045 ± 0.017	$\Lambda_b^0 \to \Lambda_c^+ \ell^- \overline{\nu_\ell}$	0.105	0.077 ± 0.018
Ξ_c^0	0.080		Ξ_b^-	0.105	
Ξ_c^+	0.080		Ξ_b^0	0.105	
Ω_c^0	0.080		Ω_b^-	0.105	

Heavy flavor hadron semileptonic decays

$\mathrm{BR}(b \to \ell^- \overline{\nu_\ell} X)$	0.1056 ± 0.0021
$\mathrm{BR}(b \to c \to \ell^+ \nu_\ell X)$	0.0801 ± 0.0026
$\mathrm{BR}(b \to \bar{c} \to \ell^- \overline{\nu_\ell} X)$	$0.0162 \pm^{0.0044}_{0.0036}$
$\mathrm{BR}(c \to \ell^+ \nu_\ell X)$	0.098 ± 0.005

Production rates

***b*-hadrons**			***c*-hadrons**		
f_{B_s}	0.117	0.107 ± 0.011	f_{D_s}	0.116	0.101 ± 0.009
$f_{b-\mathrm{baryon}}$	0.087	0.099 ± 0.017	$f_{c-\mathrm{baryon}}$	0.082	0.076 ± 0.007
$f_{B_d} = f_{B^+}$	0.398	0.397 ± 0.010	f_{D^+}	0.193	0.232 ± 0.010
			f_{D^0}	0.607	0.549 ± 0.023

3.5.1 B^0-$\overline{B^0}$ mixing

In 1986, the UA1 Collaboration at CERN observed in p-$\bar{\mathrm{p}}$ collisions an excess of events attributed to B^0-$\overline{B^0}$ mixing [33]. A neutral meson transformation into its antiparticle occurs via flavour-changing weak interactions. According to the SM, B^0-$\overline{B^0}$ transitions occur through second order weak interactions described by box diagrams involving virtual top quarks [34]. Since the energy of the collision is large enough to produce both B_d^0 and B_s^0, without identification of the meson species, the measured quantity is the average mixing parameter, $\overline{\chi}$, defined as

$$\overline{\chi} = \frac{\mathrm{BR}(b \to \overline{B^0} \to B^0 \to \ell^+ X)}{\mathrm{BR}(b \to \ell^\pm X)} \tag{7}$$

$\overline{\chi}$ is related to χ_d and χ_s, designating time-integrated mixing probabilities in the B_b^0 and B_s^0 systems respectively, as

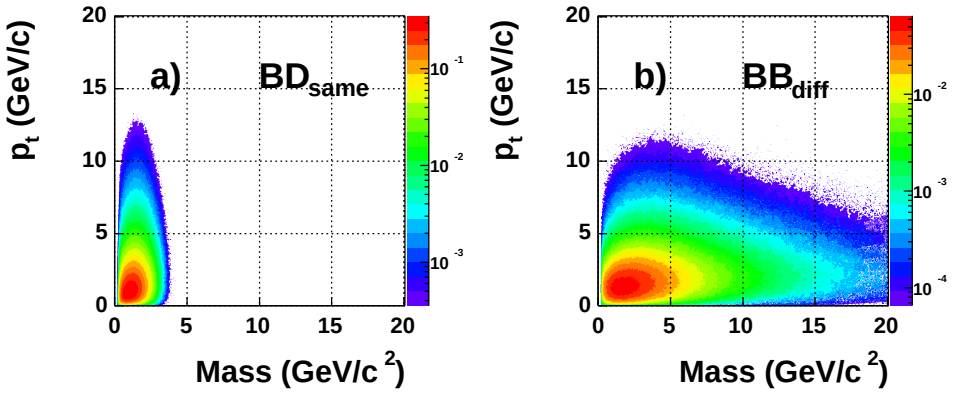

Fig. 8: b decay configurations: (a) collinear muon configuration of large transverse momentum and low mass muon pairs from the semileptonic chain decay of a single heavy b quark ($\mathrm{BD_{same}}$). (b) Dimuon events produced from semileptonic decay of both b quarks made of large mass and large transverse momentum anticollinear muons.

$$\overline{\chi} = f_{\mathrm{d}}\,\chi_{\mathrm{d}} + f_{\mathrm{s}}\,\chi_{\mathrm{s}}, \tag{8}$$

where f_{d} and f_{s} are the repective fractions of B^0_{d} and B^0_{s} in the admixture of beauty hadrons. $\overline{\chi}$ average inferred from SLD and LEP data [35] is 0.1194 ± 0.0043. A $B^0_{\mathrm{d}}\overline{B^0_{\mathrm{d}}}$ ($B^0_{\mathrm{s}}\overline{B^0_{\mathrm{s}}}$) pair then produces, in the primary dilepton channel, $\simeq 70\%$ ($\simeq 50\%$) of opposite sign correlated lepton pairs and $\simeq 30\%$ ($\simeq 50\%$) of same sign correlated lepton pairs.

More generally, $\overline{\chi}$ is related to the background subtracted ratio $\mathcal{R}$ of the number of same-sign ($\mathcal{N}_{\mathrm{SS}}$) to opposite-sign ($\mathcal{N}_{\mathrm{OS}}$) muon pairs from b-hadrons decays as follows:

$$\mathcal{R} = \frac{\mathcal{N}_{\mathrm{SS}}}{\mathcal{N}_{\mathrm{OS}}} = \frac{\mathcal{N}_{\ell^+\ell^+} + \mathcal{N}_{\ell^-\ell^-}}{\mathcal{N}_{\ell^+\ell^-}} \tag{9}$$

where,

$$\begin{aligned}
\mathcal{N}_{\mathrm{SS}} &= \mathcal{F}_{B^0\overline{B^0}} \left\{ 2\overline{\chi}(1-\overline{\chi})\,\mathcal{K}_{\mathrm{BB_{diff}}} + \left[(1-\overline{\chi})^2 + \overline{\chi}^2\right]\,\mathcal{K}_{\mathrm{BD_{diff}}} + 2\overline{\chi}(1-\overline{\chi})\,\mathcal{K}_{\mathrm{DD_{diff}}} \right\} \\
&+ \mathcal{F}_{B^+B^-}\,\mathcal{K}_{\mathrm{BD_{diff}}} \\
&+ \mathcal{F}_{B^\pm B^0}\,[\overline{\chi}\,\mathcal{K}_{\mathrm{BB_{diff}}} + (1-\overline{\chi})\,\mathcal{K}_{\mathrm{BD_{diff}}} + \overline{\chi}\,\mathcal{K}_{\mathrm{DD_{diff}}}], \\
\mathcal{N}_{\mathrm{OS}} &= \mathcal{F}_{B^0\overline{B^0}}\,\left\{ \left[(1-\overline{\chi})^2 + \overline{\chi}^2\right]\,\mathcal{K}_{\mathrm{BB_{diff}}} + 2\overline{\chi}(1-\overline{\chi})\,\mathcal{K}_{\mathrm{BD_{diff}}} + \left[(1-\overline{\chi})^2 + \overline{\chi}^2\right]\,\mathcal{K}_{\mathrm{DD_{diff}}} \right\} \\
&+ \mathcal{F}_{B^\pm B^0}\,[(1-\chi)\,\mathcal{K}_{\mathrm{BB_{diff}}} + \chi\,\mathcal{K}_{\mathrm{BD_{diff}}} + (1-\chi)\,\mathcal{K}_{\mathrm{DD_{diff}}}] \\
&+ \mathcal{K}_{\mathrm{BD_{same}}}
\end{aligned} \tag{10}$$

where $\mathcal{F}^0_B\overline{B^0}$, $\mathcal{F}_{B^+B^-}$, and $\mathcal{F}_{B^\pm\overline{B^0}}$ are the relative production fractions of $B^0\overline{B^0}$, B^+B^-, and $B^\pm\overline{B^0}$ pairs respectively. $\mathcal{F}_{\mathrm{i}}$ values extracted from PYTHIA are:

$$\begin{aligned} \mathcal{F}_{B^0\overline{B^0}} &= 0.277 \\ \mathcal{F}_{B^+B^-} &= 0.221 \\ \mathcal{F}_{B^\pm B^0} &= 0.502 \end{aligned} \tag{11}$$

$\mathcal{K}_i$ denote the fractional contributions to the final event sample from each of the muon pair classes as defined in section 3.5. A value $\mathcal{R} = 0.146$ is estimated from Monte Carlo.

3.5.2 Decays-in-flight of pions and kaons

Background originates from kaon and pion decays in flight. Primary $\pi^\pm$, $K^\pm$ are generated according to η and p_t parametrization of the distributions taken from central Pb-Pb collisions simulated using the HIJING Monte Carlo program [29] including shadowing and jet quenching (cf. Fig. 9). Central multiplicity $dN/d\eta|_{\eta=0}$ is normalized to 8000. Produced mesons are subsequently decayed to muons with the JETSET package [36]. Mid-rapidity charged particle multiplicities used in our analysis are much larger than RHIC measurements extrapolation to LHC energy, which give an estimate of $dN/dy = 1100 \div 2600$ [37]. Considering the uncertainty in extrapolating from RHIC to LHC energy, the strategy of assuming a higher particle density, adopted by all ALICE subdetectors, is a conservative approach and represents an upper feasibility limit for beauty detection.

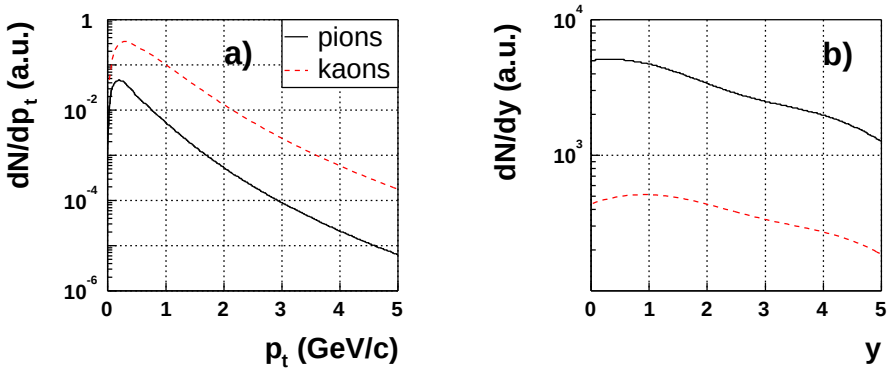

Fig. 9: Muon (a) p_t and (b) rapidity originating from decays in flight of kaons and pions.

Due to a long lifetime ($c\tau \simeq 4 \div 8$ m) and an additional Lorentz boost, π/K are most of the time absorbed by the front absorber before decaying, however the fraction that decays to muons before the absorber entry will combine with heavy flavor decays to form a large combinatorial background to be subtracted with a suitable technique (cf. section 3.6.1).

3.5.3 Resulting single muon cocktail per central collision

Fig. 10 shows the number of muons per central Pb-Pb event detected in the forward spectrometer ($2.5 < \eta^\mu < 4$) with the low trigger cut as a function of their minimum transverse momentum. Below a transverse momentum of ~ 1.5 GeV/c, contributions from charm and decay muons dominate while at larger transverse momentum beauty decays become the largest source.

As we can see in Fig. 10, a large sample of B events will be collected using an inclusive muon trigger. Single muon trigger rates are nevertheless limited by the DAQ bandwidth which

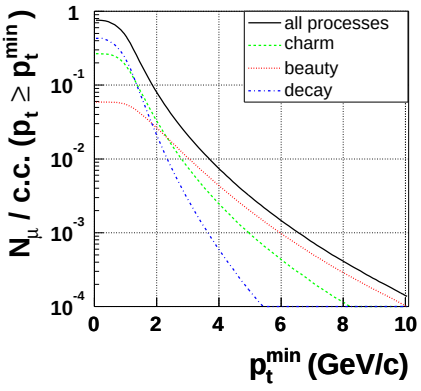

Fig. 10: Number of muons above a threshold $p_{\rm t}^{\rm min}$ per central Pb-Pb collision (5 % centrality) detected in the muon spectrometer including the low trigger cut-off.

is about 1 kHz for dimuon events in Pb-Pb collisions. In the following, we consider that the 400 Hz of 5 % most central Pb-Pb collisions are entirely put on tape. If this is not possible, corresponding prescaling factors can be used to limit the recording rate.

3.6 Measurement of heavy hadron production in muon data

In the following, we detail the method to measure the inclusive b-meson production cross section. Such an analysis was successfully implemented in past p-$\bar{\rm p}$ experiments [38]. It can be broken up into four different steps:

i. Separate the b-quark signal from backgrounds in the data sets.

ii. Measure the muon level cross section from the number of $B \rightarrow \mu$ events observed for each data set (described below);

iii. Unfold $B \rightarrow \mu$ effects from the muon level measurements to obtain the inclusive b-hadron production cross sections for the data sets, each set covering a specific b-hadron $p_{\rm t}$ region;

iv. Extrapolate the above cross sections to all $p_{\rm t}^B$ to infer the total inclusive cross section.

Actually, cross sections measured by the ALICE muon spectrometer are not strictly inclusive since muons are detected only for $2.5 < \eta^\mu < 4$ which means that b-hadron production is also measured in this range. Cross sections are then extrapolated to all rapidities using the $\mathcal{O}(\alpha_{\rm S}^3)$ predictions from Mangano, Nason, and Ridolfi.

In this analysis, the following three muon sets are used to measure heavy quark production:

- Low mass dimuons or b-chain decays ($\rm BD_{same}$) - a dimuon sample of $\rm M_{\mu\mu} < 5\,GeV/c^2$ made of muons originating from a single b-quark decay through $b \rightarrow c\mu^- \rightarrow \mu^+$;
- High mass dimuons - a dimuon sample with $5 < \rm M_{\mu\mu} < 20\,GeV/c^2$ sensitive to $b\bar{b} \rightarrow \mu^+\mu^-$, each muon coming from a different quark in the pair ($\rm BB_{diff}$);
- Inclusive single muon sample.

3.6.1 Background subtraction

Subtracting the background to the S + B spectrum is essential for extracting a signal from heavy flavor semileptonic decays when the signal is small and/or when the shape of the background is unknown. The usual technique for background subtraction consists in estimating the uncorrelated background in the unlike-sign pair sample by the measured distribution of like-sign pairs. Whereas this method has been successfully applied in dilepton physics at SPS energies [39, 40, 41], its applicability at the LHC is questionable because the combinatorial background contains a sizeable fraction of leptons from B mesons decay. Indeed, a $B\overline{B}$ pair produces not only unlike-sign correlated lepton pairs, but also like-sign correlated lepton pairs due to cascade decays and B^0-$\overline{B^0}$ oscillations as explained in section 3.5.

Due to these effects the unlike-sign dilepton spectrum does not contain the full correlated signal because a part of this correlated signal is made of like-sign lepton pairs. Consequently, the like-sign subtraction removes from the unlike-sign dilepton spectrum not only the uncorrelated component but also a fraction of the correlated signal. This could tremendously bias the estimation of the continuum yield. We note that the problem can be overcome by using other methods for background subtraction such as the so-called event-mixing. Although the event-mixing method has its own drawbacks, it is not affected by the effect discussed above and it should give a reliable estimate of the combinatorial background as demonstrated in section 3.6.4.

In the following, we assume that the background can be subtracted perfectly *i.e.* without any systematic bias (therefore, the statistical error of the full spectra is simply propagated to the correlated spectra). This surely corresponds to an ideal case. A precise determination of possible systematic uncertainties related to the background subtraction with the event-mixing technique will have to be determined by means of full simulations. In particular, different centralities of the mixed events as well as two track resolution of the apparatus, which are known to be potentially responsible for biases, must be investigated carrefully.

3.6.2 Single muon transverse momentum cut-off optimization

Charm and beauty are produced at large transverse momentum with similar rates but the harder beauty fragmentation results in a harder transverse momentum spectrum of muons. Applying a muon $p_{\rm t}$ cut thus enriches the selected muon samples in $b\bar{b}$ decays relative to $c\bar{c}$ decays. This can be observed from the inspection of Fig. 11 which shows signal, signal to background ratio and significance for charm and beauty decay muons as a function of a $p_{\rm t}$ threshold on single muons. In the following analysis, a conservative $p_{\rm t}$ threshold of 1.5 GeV/c was applied to define a clean sample of muons from beauty decay. Such a threshold allows to select a large beauty signal with relatively good signal to background ratio and optimum significance (as mentionned before, such a cut is also mandatory in order to get rid of the trigger inefficiency at low $p_{\rm t}$). Note that, if one can afford to work with a reduced signal depending on the physics goals of the analyses, this sample could be further enriched in muons from beauty decay by pushing the $p_{\rm t}$ threshold to 2 GeV/c. By doing so the beauty fraction in enhanced by a factor ~ 1.5 while the significance remain unchanged.

A similar transverse momentum threshold can be applied to the dimuon data sample. As shown in Fig. 12, the b signal fraction[5] reach 80 % of the correlated heavy quark data both in the low and high mass regions. Besides, it is worth noting that a further increase in the transverse momentum threshold to values as high as 3 GeV/c only slightly enhances the beauty fraction (by 10 % in the low mass region while remains unchange in the high mass region) while exhausting

[5] $\mathrm{f}_{b\bar{b}} = \mathrm{N}_{b\bar{b}}/(\mathrm{N}_{b\bar{b}} + \mathrm{N}_{c\bar{c}})$.

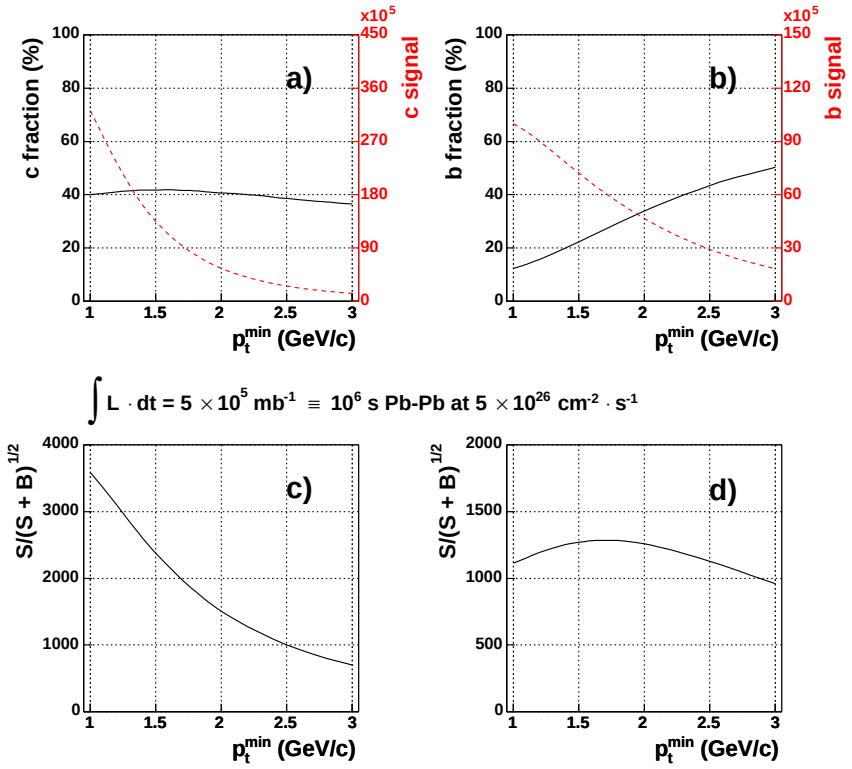

Fig. 11: Signal (dashed line, right scale), signal to background ratio (solid line, left scale), and significance for (a) and c)) charm and beauty (b) and d)) decay muons (5 % most central collisions). The 1 GeV/c $p_{\rm t}$ threshold corresponds to the low trigger cut-off while higher values include an additional sharp cut.

the available statistics. Thus, a transverse momentum threshold higher than 1.5 GeV/c is not mandatory for beauty exclusive analysis even if it could reduce drastically the combinatorial background and then decrease statistical errors on the measured signal.

3.6.3 Muon data sets

Muon samples used in this analysis have a common transverse momentum cut-off of 1.5 GeV/c (see previous section) and are emitted in the spectrometer rapidity window. An additional mass cut allows to define two different mass regions sensitive to distinct processes.

High-mass dimuon sample

High mass muon pairs (coming from different b-quarks) defined to have $\mathrm{M}_{\mu\mu} > 5\,\mathrm{GeV/c^2}$ are selected with the following physics cuts:

$$\begin{aligned} 1.5\,\mathrm{GeV/c} &< p_{\rm t}^{\mu} \\ 2.5 &< \eta^{\mu} < 4 \\ 5 &< \mathrm{M}_{\mu^+\mu^-} < 20\,\mathrm{GeV/c^2} \end{aligned}$$

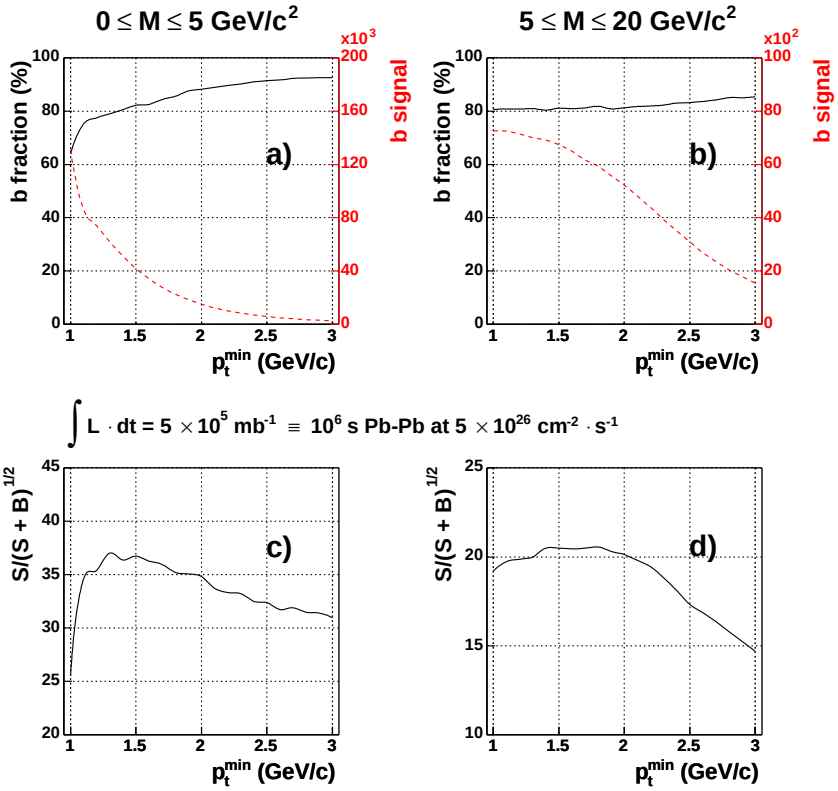

Fig. 12: Signal (dashed line, right scale), signal to background ratio (solid line, left scale), and significance for opposite sign muon pairs from beauty decays of invariant mass below 5 GeV/c^2 (a) and c)) and above (b) and d)).

Low-mass dimuon sample

Low mass dimuons are selected applying the following physics cuts:

$$\begin{aligned} 1.5\,\mathrm{GeV/c} &< p_{\mathrm{t}}^{\mu} \\ 2.5 < \eta^{\mu} &< 4 \\ \mathrm{M}_{\mu^+\mu^-} &< 5\,\mathrm{GeV/c^2} \end{aligned}$$

This data set contains 5×10^4 signal events originating mainly from b-chain decays

Inclusive muon sample

Single muon data is defined by the following physics cuts:

$$\begin{aligned} p_{\mathrm{t}}^{\mu} &> 1.5\,\mathrm{GeV/c} \\ 2.5 < \eta^{\mu} &< 4 \end{aligned}$$

The inclusive single muon sample is of large statistics, containing roughly 3×10^7 events which come from semi-muonic decay of heavy quarks and decay background.

3.6.4 Extracting the *b*-fraction

ALICE forward muon spectrometer unlike other instruments [42, 43, 44] is not equipped to discriminate $b\bar{b}$ events from background on an event-by-event basis. Instead the fraction of $b\bar{b}$ events can be assessed on a statistical basis. Applying a cut-off on the transverse momentum of single muons remains the only useful quantity to provide a rejection of background processes (namely open charm). As seen in section 3.6.2, a muon transverse momentum of 1.5 GeV/c is enough to maximise the *b*-signal significance over the entire mass range. In order to discriminate between the $b\bar{b}$ signal and the $c\bar{c}$, we use Monte Carlo predicted mass shapes for $b\bar{b}$ and $c\bar{c}$ fitted to the data. Variables chosen to perform chi-square fits are the dimuon mass and the single muon transverse momentum with process amplitudes $\mathcal{A}_i$ as free parameters. A normalization constrain is imposed, namely $\sum_i \mathcal{A}_i = 1$, such that only one parameter (beauty amplitude) is needed for dimuon mass fits and two parameters (charm and beauty amplitudes) for inclusive fits. Resulting amplitudes of the various physics processes are given in Table 7 and 8. Note the large value of the χ^2 of the single muon transverse momentum fit which does not come from a bad hypothesis on probablity distribution functions used to fit data points but rather from very small measurement errors σ_i due to the very large statistics accumulated.

Table 7: Fitted dimuon beauty fractions in the low and high mass regions. Errors are systematic due to the fitting procedure. Correponding number of events and cross sections are quoted as well.

	$2\,m_\mu < M_{\mu^+\mu^-} < 5\,GeV/c^2$	$5 < M_{\mu^+\mu^-} < 20\,GeV/c^2$
$f_{b\bar{b}}$	0.835 ± 0.015	0.822 ± 0.016
χ^2_{fit}	31/34 d.o.f.	35/44 d.o.f.
$N_{b\bar{b}}$	41461 ± 793	6983 ± 130
$\sigma^{\mu^+\mu^-}$ [μb]	130.380 ± 2.494	19.317 ± 0.360

Table 8: Measured *b* fraction in the inclusive single muon data set. Corresponding number of *b* events and muon cross sections are also calculated including uncertainty from the fit only.

	$1.5 < p_t^\mu < 3\,GeV/c$	$3 < p_t^\mu < 6\,GeV/c$	$6 < p_t^\mu < 9\,GeV/c$	$9 < p_t^\mu < 30\,GeV/c$
f_b	0.223 ± 0.0002			
χ^2_{fit}	2792/183 d.o.f.			
N_b	5360350 ± 1439	1659150 ± 445	143444 ± 38	30368 ± 8
σ^μ [μb]	12583 ± 3.377	3691.1 ± 0.990	316.304 ± 0.085	65.098 ± 0.017

Opposite sign muon pairs

Resultant fit to the opposite sign dimuon mass spectra is shown in Fig. 13. Statistical errors quoted account for the background subtraction method *i.e.* the uncorrelated background is subtracted on average but statistical fluctuations are still the ones of the combinatorial background. In the high mass region, due to similar shapes, the charm content has been fixed to the value fitted in the low mass region where the forms of the p.d.f are very different.

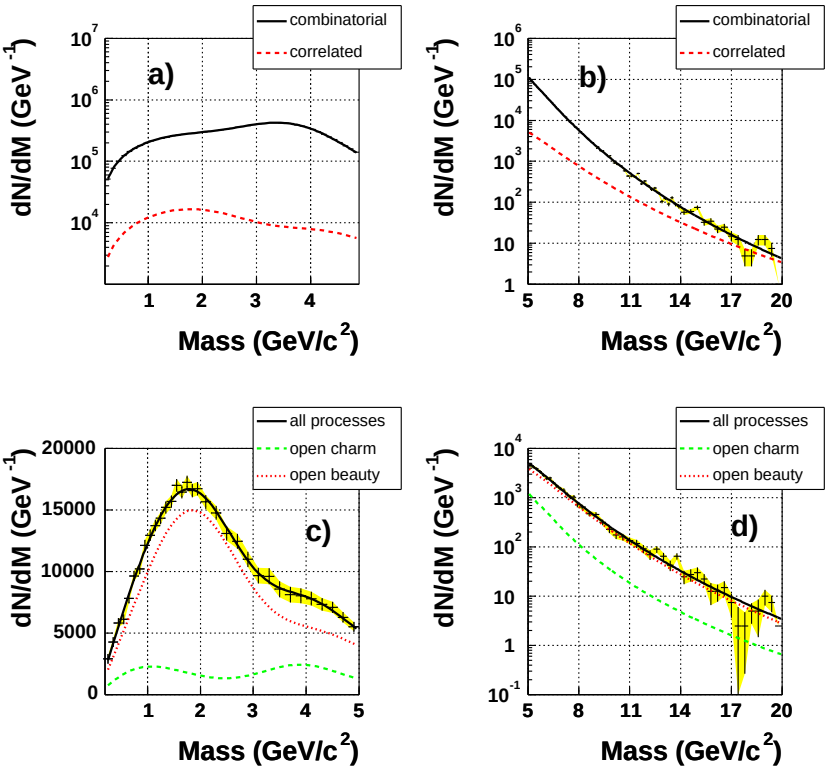

Fig. 13: Invariant mass distributions of $\mu^+\mu^-$ pairs produced in central Pb-Pb collisions at 5.5 TeV in the low (left panels) and high mass regions (right panels). A $p_t > 1.5$ GeV/c cut-off has been applied to muon tracks. Top panels show the contribution of the combinatorial background (black solid line) including the correlated signal (red dotted line) made of a muon pair originating from the decay of the same initial $b\bar{b}$ pair. Background subtracted mass spectra are presented in bottom panels. Charm and beauty signal are plotted in green and red line respectively.

Concerning open charm production, simultaneous requirements of a large transverse momentum for each muon and a low dimuon mass (cf. Fig. 13(c)) imply a sizeable transverse momentum of the dimuon system typical of NLO topologies.

Same sign muon pairs

Correlated same sign dimuons shown in Fig. 14 are essentially due to beauty decays when one of the b meson from the produced pair oscillates into its anti-particle. As demontrated in section 3.5.1, the correlated same sign component from beauty is related to the opposite sign signal such that the same sign sample can be used as a cross check to the opposite sign measurement. The yield of like-sign correlated lepton pairs from beauty decay [46] is obtained by subtracting the event-mixing distribution from the like-sign distribution. This measurement suffers from large statistical errors in the low mass region where the signal-to-background ratio is particularly small (S/B $\simeq$ 1/200). The same sign meaurement gets more precise in the high mass region where the contribution from the combinatorial background decreases.

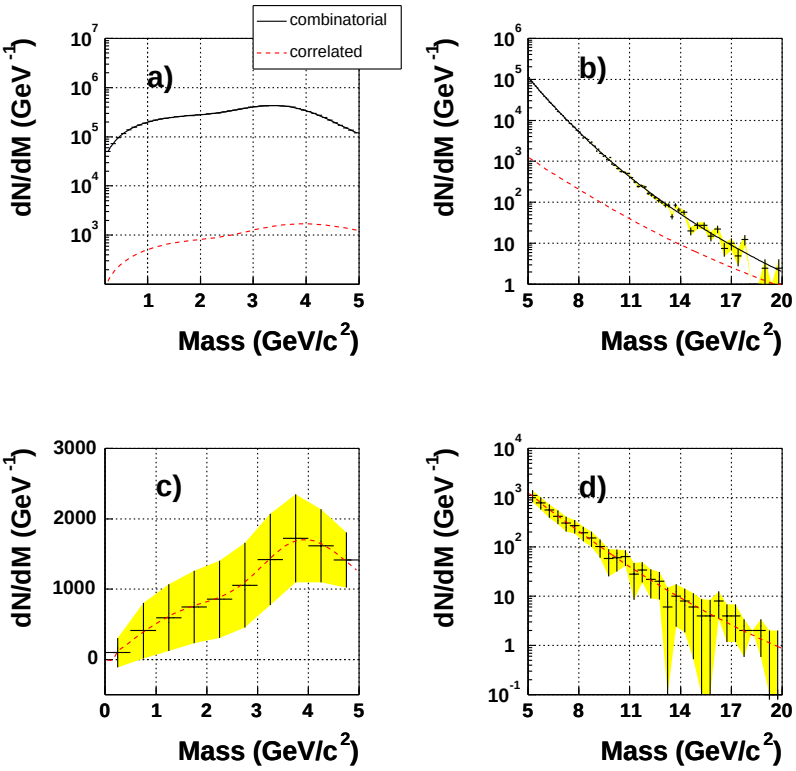

Fig. 14: Invariant mass spectra of $\mu^{\pm}\mu^{\pm}$ pairs. A $p_{\rm t} > 1.5\,{\rm GeV/c}$ cut-off was applied to muon tracks. a) and b) panels show the contributions from combinatorial (solid line) and correlated components (dashed line) in the low and high mass region, respectively. c) and d) plots are the background subtracted signals from beauty decays. Errors are statistical only for one month of central Pb-Pb collisions.

Single muons

The inclusive muon $p_{\rm t}$ distribution simulated from $1.5\,{\rm GeV/c}$ to $20\,{\rm GeV/c}$ is shown in Fig 15. $p_{\rm t}$-integrated fitted b fraction accounts only for 0.223 ± 0.0002 of the data sample while main contributions come from charm and π/K decays due to high low $p_{\rm t}$ rates. Increasing the $p_{\rm t}$ threshold could greatly enhance the beauty fraction.

3.6.5 Muon level cross sections

After having determined the number of b events in the three data samples calculated from the fitted b and $b\bar{b}$ fractions, these numbers can be converted into cross sections by simply dividing by the integrated luminosity ($5 \times 10^5\,{\rm mb}^{-1}$). One can note that such cross sections could be directly compared to other experimental results since they reflect the basic characteristics of the data samples containing only cuts on "universal" quantities namely $p_{\rm t}$ and $\rm M_{\mu\mu}$. Cross sections should be corrected for global efficiencies ε (given in Table 5) such that finally they can be expressed as

$$\sigma^{\mu} = \frac{\rm N_b}{\int \mathscr{L}\,{\rm d}t} \times \frac{1}{\varepsilon} \qquad (12)$$

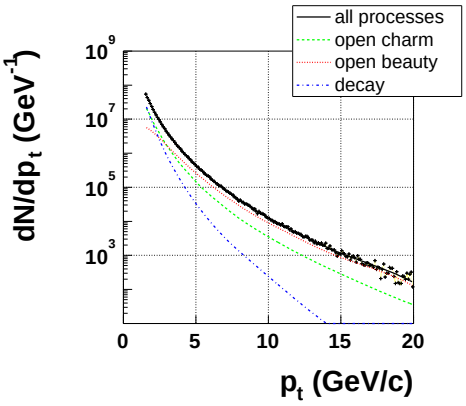

Fig. 15: Inclusive muon transverse momentum distribution based on one month (10^6 s) Pb-Pb data taking for the 5 % most central collisions.

where N_b is the number of b events extracted from the fit. Muon level cross sections for each data sample are quoted in Table 7 and 8. Systematic errors that should be taken into account when calculating the muon level cross section are listed in Table 11, they essentially account for the uncertainties on the luminosity and the efficiency correction.

3.6.6 Inclusive *b*-hadron production cross section

Experimentally, muon cross section (σ^{μ}) are measured, in order to compute b-hadron production cross section, the muon yields has to be disentangled from branching ratios and decay kinematics. Extensively studied in experiments at e^+e^- colliders, B decay is relatively well understood [47, 48, 49, 50]. A Monte Carlo method [38] is used to extrapolate the muon level cross section into a b-hadron level cross section. In order to eliminate potential bias in the unfolding procedure due to non-pertubative hadronization effects[6], we have chosen to present b-hadron instead of b-quark production cross section as recommended in Ref. [51]. Measured b-hadron cross section is obtained by scaling the muon level (σ^{μ}) by the predicted Monte Carlo cross section ratio as

$$\begin{aligned} \sigma^B\,(\,p_{\rm t}^B > p_{\rm t}^{\rm min}\,) &= \sigma^{\mu} \times \left.\frac{\sigma^B\,(\,p_{\rm t}^B > p_{\rm t}^{\rm min}\,)}{\sigma^B(\Phi^{\mu})}\right|_{\rm MC} \\ &= \sigma^{\mu} \times \mathcal{F}_{\mu\to B}, \end{aligned} \tag{13}$$

where:

- $\sigma^B\,(\,p_{\rm t}^B > p_{\rm t}^{\rm min}\,)$ is the integral of the transverse momentum spectrum of b-hadrons with rapidity $2.5 < y^B < 4$ and $p_{\rm t}^B > p_{\rm t}^{\rm min}$.
- and $\sigma^B(\Phi^{\mu})$ is the integral of the transverse momentum distribution of b-hadrons decaying into muons within a given phase space Φ^{μ} ($\rm M_{\mu\mu}$ range, $2.5 < y^{\mu} < 4$ and/or $p_{\rm t}^{\mu}$ cut-off). $p_{\rm t}^{\rm min}$ is defined such that 90 % of the accepted B-hadrons had a transverse momentum larger than that value (see Fig. 16).

[6] Bias that could explain part of the observed discrepancy between CDF and D0 beauty quark hadroproduction cross section measurements and NLO in QCD predictions [45]

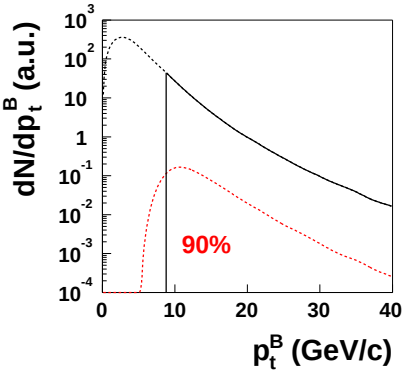

Fig. 16: Sketch of differential cross sections ($\mathrm{d}N/\mathrm{d}p_{\mathrm{t}}^{B}$) for inclusive b-hadron production (solid line) and for those b-events which yield a muon of $p_{\mathrm{t}} > 6\,\mathrm{GeV/c}$ (dashed line).

In the $B \to \mu$ decay, muons are generally produced with $p_{\mathrm{t}}^{\mu} < p_{\mathrm{t}}^{B}$ (cf. Fig. 17). Muon p_{t} cuts in each data sample are therefore also effective B p_{t} cuts, and B production cross sections measured at the muon level extend from some minimum p_{t}^{B} (defined as $p_{\mathrm{t}}^{\mathrm{min}}$) to the maximum kinematically possible.

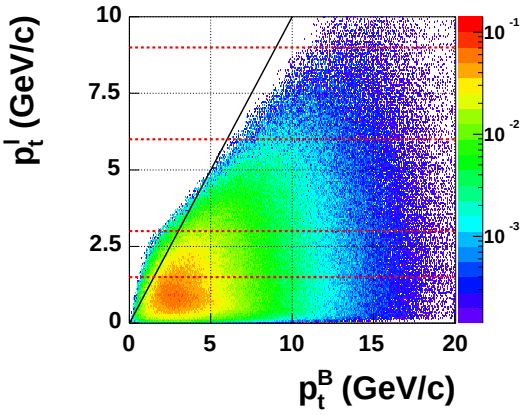

Fig. 17: Correlation between the muon transverse momentum and its parent b-hadron. Second generation decay muons are included. Horizontal dashed lines indicate the limits of the inclusive single muon transverse momentum bins.

Computed values of $p_{\mathrm{t}}^{\mathrm{min}}$ and $\mathcal{F}_{\mu \to B}$ are listed in Table 9 and 10. Final b-hadron cross sections are plotted in Fig. 18.

3.7 Source of systematics

Systematic uncertainties enter both the calculation of muon cross sections σ^{μ} and conversion factors $\mathcal{F}$. Major sources of systematic errors to be taken into account are listed in Table 11. Systematic uncertainties has to be evaluated carefully requiring intense Monte Carlo computing

Table 9: Conversion factors of inclusive single muon cross sections into b-hadron cross sections.

$p_{\rm t}^{\mu}$ (GeV/c)	$p_{\rm t}^{\rm min}$ (GeV/c)	$\mathcal{F}_{\mu\to B}$
$1.5 \div 3$	2.35	30.500
$3 \div 6$	4.20	54.255
$6 \div 9$	8.80	94.579
$9 \div 30$	13.65	83.359

Table 10: Conversion factors of dimuon muon cross sections into b-hadron cross sections.

$\mathrm{M}_{\mu^+\mu^-}$ (GeV/c^2)	$p_{\rm t}^{\rm min}$ (GeV/c^2)	$\mathcal{F}_{\mu\to B}$
$2\,\mathrm{m}_{\mu} \div 5$	2.05	3.079
$5 \div 20$	2.85	16.628

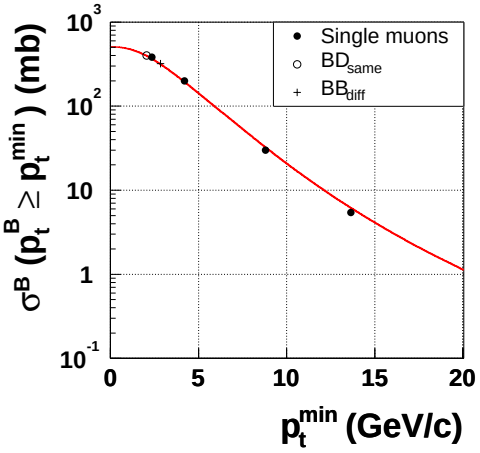

Fig. 18: Inclusive b-hadron cross section in $2.5 < y^B < 4$ as a function of $p_{\rm t}^{\rm min}$. Also shown the PYTHIA prediction (red line) used to produce the signal.

efforts and is clearly beyond the scope of the present note. Here, we limit ourselves to quote the integrated b-quark production cross section as a function of the minimum transverse momentum threshold including only (small) systematics due to the fitting procedure.

4 Conclusion

In this note, we have presented the results of the analysis of b-hadron production measurement using muon detection in the ALICE forward spectrometer. The measurement of b production provides an important test of the theory of QCD in heavy ion collisions where new effects are expected as compared to simple nucleon-nucleon interactions. A precise measurement of the inclusive $\mathrm{d}\,\sigma^B/\mathrm{d}\,p_{\rm t}$ cross section will allow to probe in-medium effects known to be $p_{\rm t}$-dependent.

Table 11: Systematic errors associated with the calculation of the inclusive B production cross section.

	Source
σ^{μ}	
	$\int \mathscr{L}\,\mathrm{d}t$
	ε
	χ^2 fit
	Background subtraction
$\mathcal{F}_{\mu\to b}$	
	$\mathrm{BR}\,(b \to \mu\, X)$
	Muon spectrum $b \to \mu X$

Our ability to measure b-hadrons down to very low transverse momentum (2.5 GeV/c) in the worst conditions of central Pb-Pb collisions is furthermore a possibility to constrain pQCD calculations in a region where they are know to be less precise. Nevertheless, this analysis has to be completed by a detailed study of systematic uncertainties spoiling the measurement. Expected statistics are high so that the analysis could refined splitting data sample into $p_{\mathrm{t}}^{\mu\mu}$ or $p_{\mathrm{t}}^{\mathrm{lead}}$ bins exploring even more the inclusive cross section. Finally, azimuthal correlations contributing to QCD production mechanisms are still to be studied as a unique potentiality via dimuon detection in the muon spectrometer.

References

[1] F. Abe *et al.*, Phys. Rev. Lett. **71** (1993) 500.

[2] F. Abe *et al.*, Phys. Rev. Lett. **71** (1993) 2396.

[3] F. Abe *et al.*, Phys. Rev. Lett. **75** (1995) 1451.

[4] B. Abbott *et al.*, Phys. Lett. **B 487** (2000) 264.

[5] CDF Collaboration, D. Acosta *et al.*, Phys. Rev. **D65** (2002) 052005, `hep-ph/0111359`.

[6] M. Cacciari and P. Nason, Phys. Rev. Lett. 89 (2002) 122003.

[7] Z. w. Lin and M. Gyulassy, Phys. Rev. **C51** (1995) 2177 ; Z. w. Lin and M. Gyulassy, Phys. Rev. **C52** (1995) 2177, [Erratum-ibid. **C52** (1995) 440].

[8] Z. w. Lin and M. Gyulassy, Phys. Rev. Lett. 77 (1996) 1222.

[9] ALICE Collaboration, "ALICE Physics Theoretical Overview", ALICE Internal Note 2002-025.

[10] T. Sjöstrand, P. Edén, C. Friberg, L. Lönnblad, G. Miu, S. Mrenna and E. Norrbin, Computer Physics Commun. **135** (2001) 238.

[11] M.L. Mangano, P. Nason and G. Ridolfi, Nucl. Phys. **B 373** (1992) 295.

[12] P. Nason, S. Dawson, and R.K. Ellis, Nucl. Phys. **B 303** (1988) 607.

[13] N. Carrer and A. Dainese, `hep-ph/0311225`

[14] H. L. Lai *et al.*, Phys. Rev. **D 55** (1997) 1280.

[15] R.D. Field, Phys. Rev. **D65** (2002) 09006.

[16] M. Arneodo, Phys. Rep. **240** (1994) 301-393.

[17] K. J. Eskola, V. J. Kolhinen and C. A. Salgado, Eur. Phys. J. **C 9** (1999) 61-68.

[18] B. Andersson, G. Gustafson, G. Ingelman and T. Sjöstrand, Phys. Rep. 97 (1983) 31.

[19] C. Peterson *et al.*, Phys. Rev. **D 27** (1983) 105.

[20] G. Altarelli *et al.*, Nucl. Phys. **B 208** (1982) 365.

[21] P. Nason, S. Dawson, and R.K. Ellis, Nucl. Phys. **B327** (1989) 49.

[22] K. Adcox *et al.*, Phys. Rev. Lett. 88 (2002) 192203.

[23] E. L. Berger, Phys. Rev. **D 37**, (1988) 1810.

[24] R.J. Glauber, Lecture in Theoretical Physics, Vol. 1, eds W.E. Brittin and L.G. Dunham (Interscience, New-York, 1959) p. 315 ; in: Proc. 2nd Int. Conf. on High Energy Physics and Nuclear Structure, ed. G. Alexander (North Holland, Amsterdam, 1967) p. 311 ; in: Proc. 3rd Conf. on High Physics and Nuclear Structure, ed. S. Devons (Plenum Press, New York, 1969) p. 207.

[25] R. Vogt, Heavy Ion Phys. 9 (1999) 339.

[26] D. d'Enterria, `nucl-ex/0302016`.

[27] P. Cortese and A. De Falco, `http::://alisoft.cern.ch`.

[28] K. Boudjemline *et al.*, SUBATECH-2002-30.

[29] X. N. Wang and M. Gyulassy, Phys. Rev. **D 44**, 3501 (1991).

[30] ALEPH, CDF, DELPHI, L3, OPAL, SLD Collaborations, "Combined results on b-hadron production rates and decay properties", "A Combination of Preliminary Electroweak Measurements and Constraints on the Standard Model", prepared from contributions of the LEP and SLD experiments to the 2003 Winter Conferences, LEPEWWG/2003-01, 8 April 2003.

[31] The LEP Collaborations ALEPH, DELPHI, L3, OPAL, the LEP Electroweak Working Group and the SLD Electroweak and Heavy Flavor Group, "A Combination of Preliminary Electroweak Measurements and Constraints on the Standard Model", LEPEWWG/2004-01, 6 December 2004.

[32] K. Hagiwara *et al.*, Phys. Rev. **D 66** (2002) 010001.

[33] UA1 Collaboration, "Search for B^0-$\overline{B^0}$ oscillations at the CERN proton-antiproton collider", Phys. Lett. **B 186** (1987) 247.

[34] P.J. Franzini, Phys. Rep. **173** (1989) 1.

[35] The LEP Collaborations ALEPH, DELPHI, L3, OPAL, the LEP Electroweak Working Group and the SLD Heavy Flavor and Electroweak Groups, "A Combination of Preliminary Electroweak Measurements and Constraints on the Standard Model", prepared from contributions of the LEP and SLD experiments to the 2000 Summer Conferences, CERN-EP-2001-021.

[36] T. Sjostrand, Comput. Phys. Commun. 27 (1982) 243.

[37] ALICE Collaboration, ALICE Physics Performance Report Volume I, CERN/LHCC 2003-049, 7 November 2003.

[38] UA1 Collaboration, C. Albajar *et al.*, Phys. Lett. **B 213** (1988) 256,
UA1 Collaboration, C. Albajar *et al.*, Phys. Lett. **B 256** (1991) 121.

[39] M.C. Abreu et al., Eur. Phys. Jour. **C 14** (2000) 443

[40] G. Agakichiev et al., Phys. Lett. **B 422** (1998) 405

[41] A.L.S. Angelis et al., Eur. Phys. Jour. **C 13** (2000) 433.

[42] NA60 Collaboration, A. Baldit *et al.*, CERN/SPSC 2000-010, SPSC/P316, 7 March 2000.

[43] J. Ellison [D0 Collaboration], `hep-ex/0101048`.

[44] CDF Collaboration, F. Abe *et al.*, Nucl. Instrum. and Meth. **A 271** (1988), 387.

[45] M. Cacciari and P. Nason, Phys. Rev. Lett. 89 (2002) 122003.

[46] P. Crochet, P. Braun-Munzinger, Nucl. Instrum. and Methods **A 484** (2002) 564-572.

[47] U. Langenegger [BABAR Collaboration], `hep-ex/0402032`.

[48] K. M. Ecklund, `hep-ex/9912034`.

[49] K. Abe *et al.* [Belle Collaboration], Phys. Lett. **B 547** (2002) 181.

[50] D. Abbaneo *et al.* [ALEPH Collaboration], `hep-ex/0112028`, CERN-EP/2001-050.

[51] R. Field, "b-Quark Production at the Tevatron", talk presented at the Fermilab ME/MC Tuning Workshop, April 30, 2003.